Proc. Natl. Acad. Sci. USA
Vol. 93, pp. 1710–1715, February 1996
Neurobiology

Zn^{2+} interaction with Alzheimer amyloid β protein calcium channels

(giant amyloid β-protein channel/lipid bilayer/zinc-binding motif/zinc blockade)

NELSON ARISPE, HARVEY B. POLLARD, AND EDUARDO ROJAS

Laboratory of Cell Biology and Genetics, National Institute of Diabetes, Digestive and Kidney Diseases, National Institutes of Health, Bethesda, MD 20892

Communicated by Julius Axelrod, National Institute of Mental Health, Bethesda, MD, October 31, 1995

ABSTRACT **The Alzheimer disease 40-residue amyloid β protein (AβP[1–40]) forms cation-selective channels across acidic phospholipid bilayer membranes with spontaneous transitions over a wide range of conductances ranging from 40 to 4000 pS. Zn^{2+} has been reported to bind to AβP[1–40] with high affinity, and it has been implicated in the formation of amyloid plaques. We now report the functional consequences of such Zn^{2+} binding for the AβP[1–40] channel. Provided the AβP[1–40] channel is expressed in the low conductance (<400 pS) mode, Zn^{2+} blocks the open channel in a dose-dependent manner. For AβP[1–40] channels in the giant conductance mode (>400 pS), Zn^{2+} doses in the millimolar range were required to exert substantial blockade. The Zn^{2+} chelator *o*-phenanthroline reverses the blockade. We also found that Zn^{2+} modulates AβP[1–40] channel gating and conductance only from one side of the channel. These data are consistent with predictions of our recent molecular modeling studies on AβP[1–40] channels indicating asymmetric Zn^{2+}-AβP[1–40] interactions at the entrance to the pore.**

Alzheimer disease (AD) is a chronic dementia affecting increasingly large numbers of the aging population and is characterized pathologically by the presence of extracellular amyloid plaques in the brain and intraneuronal neurofibrillary tangles (1–3). The major component of brain amyloid plaques is a 39- to 42-residue peptide termed amyloid β protein (AβP) (4–6), which is a proteolytic product of the widely distributed amyloid precursor glycoprotein (APP_{751}), defined by a locus on chromosome 21 (7, 8). In particular, the AβP[1–40] has been linked to the neurotoxic principle causing neuronal death in the disease, although the mechanism has remained elusive (1, 9–12). However, we have shown that AβP[1–40] can incorporate into liposomes and lipid bilayer membranes and form cation-selective channels that conduct Ca^{2+} and other cations (13, 14). These channels exhibit, as a rule, several rapidly interconverting levels of conductance in both low (<400 pS) and giant (>400 pS) modalities. We also observed that the relationships between currents and transmembrane potentials (I–V curves) were linear in symmetrical conditions. We have therefore suggested that the ability of the AβP[1–40] to form these cation channels could be the molecular basis of amyloid neurotoxicity (15, 16).

In a concerted effort to understand the mechanism of AβP actions, we have recently completed a molecular modeling study which stresses the likely oligomeric nature of the AβP[1–40] channels (17). The molecular models also indicate that the channel might be intrinsically asymmetric within the membrane. This asymmetry is particularly emphasized at the putative entrances to the aqueous pore, where sites rich in histidine and anionic residues predominate. Such sites have been associated with Zn^{2+} binding in other proteins (18–24), and Zn^{2+} has been shown to bind AβP[1–40] with high affinity (25, 27, 32). We therefore hypothesized that the consequence of Zn^{2+} binding to AβP[1–40] might be an effect on the amyloid channel behavior.

We found and report here that the AβP[1–40] channel gating and conductance are indeed modulated by Zn^{2+} addition to one side of the channel. Channel conductance was reduced by Zn^{2+} in a dose-dependent manner, complete blockade being achieved only if the amyloid peptide channel conductance occurred in the low pS range (13). If the AβP[1–40] channel activity was in the giant nS range (14), millimolar doses of Zn^{2+} were required to induce a significant reduction in conductance. Changes in channel conductance induced by Zn^{2+} binding were not voltage dependent, and *o*-phenanthroline, a Zn^{2+} complexing agent, reversed all observable Zn^{2+} effects on AβP[1–40] channel activity. From these data we conclude that the AβP[1–40] conformation in the negatively charged lipid bilayer allows interactions between Zn^{2+} and AβP[1–40], probably at a binding site proximal to the pore.

METHODS

The methods used here have been previously described (13, 14). In brief, the AβP[1–40] peptide, obtained from Bachem, was dissolved in water at a concentration of 0.46 mM. AβP[1–40] channel incorporation into acidic phospholipid planar bilayer membranes was achieved either directly from the solution or indirectly by fusion of pure phosphatidylserine liposomes, which were prepared by sonication of the liposomes in the presence β-amyloid (13). The experimental chamber consisted of two compartments (capacity *ca.* 1 cm^3 each), separated by a thin Teflon film with a small circular hole (50–100 μm) at the center. Planar bilayers were formed by spreading on the hole a mixture of POPE and phosphatidylserine (50 mg/cm^3) dissolved in decane. For channel studies, 5 μl of the liposome preparation containing the AβP peptide (*ca.* 5 μM AβP) was added to the side of the chamber electrically connected to the input of the voltage-clamp amplifier (cis). Single channel currents were recorded using a patch clamp amplifier (Axopatch-1D) equipped with a low noise headstage (CV-4B) specially designed for black lipid membrane work. Permanent records of the current and transmembrane potential were made on magnetic tape using a PCM/VCR digital system. The analysis of the records was made from playbacks through a lowpass filter set in the range from 200–500 Hz. We selected those records which exhibited single AβP[1–40] channel events. Since several current levels were observed in the majority of the AβP[1–40] channel records, fulfillment of this criterium entailed detection of spontaneous transitions between extreme levels of current, ideally complete channel closures from the maximum. The electrical potential of the solution in the cis compartment is referenced to that in the trans compartment which is electrically

The publication costs of this article were defrayed in part by page charge payment. This article must therefore be hereby marked "*advertisement*" in accordance with 18 U.S.C. §1734 solely to indicate this fact.

Abbreviations: AD, Alzheimer disease; AβP, amyloid β protein; I–V, current–voltage; FT, fractional time.

connected to ground. Positive charge moving through the open channel from the trans to the cis side represents negative current.

For the experiments reported here the same solution was used to fill both compartments of the bilayer chamber. These consisted of symmetrical KCl solutions (in mM; 40 KCl, 3 KHepes, and 0.3 $CaCl_2$, pH 7.4, and 140 KCl, 3 KHepes, and 0.3 $CaCl_2$, pH 7.4) or CsCl solutions (in mM: 40 CsCl, 3 CsHepes, and 0.3 $CaCl_2$, pH 7.4). A few experiments were also conducted using symmetrical Cs glutamate solutions (in mM: 190 Cs glutamate and 10 CsPipes, pH 7.6).

RESULTS

Demonstration of Direct Interactions Between Zn^{2+} and AβP[1–40] Channels of Low Conductance (<400 pS). To detect any possible interactions between Zn^{2+} and AβP[1–40] channel molecules, we reconstituted the AβP[1–40] channel activity by fusing unilamellar liposomes containing the AβP with the bilayer (13). Fig. 1 depicts six segments of a continuous record of AβP channel activity recorded in symmetrical CsCl solutions. Control records acquired prior to the application of Zn^{2+} illustrate the activity of the AβP[1–40] channel at different transmembrane potentials from −40 to 40 mV (Fig. 1*A*). These data are consistent with our previous observations indicating that with Cs^+ as the charge carrier in a symmetrical system, a single level of conductance was frequently present. In the example shown in Fig. 1*C*, this conductance was 110 pS, exhibiting infrequent closures over the voltage range examined (i.e., from −40 to 40 mV; Fig. 1*A*). However, as depicted in Fig. 1*B*, addition of Zn^{2+} (250 μM) to both sides of the bilayer induced a profound change in the AβP[1–40] channel activity. Several new levels of current were seen, and frequent transitions occurred between different lower levels of conductance. The most frequent levels of conductance observed were *ca.* 82, 44, and 19 pS (Fig. 1*C*, □). A few minutes after the removal of Zn^{2+} from one of the sides (the trans side), these effects were reversed and the conductance returned to 108 pS, a value close to the control level of 110 pS (Fig. 1*C*, ■). This indicated that the Zn^{2+} ions present in the other side (the cis side) were not responsible for the observed effects.

In the presence of Zn^{2+} (250 μM) the AβP[1–40] channel activity, depicted in Fig. 2 at −40 mV on an expanded time base, clearly shows the presence of brief transitions between different levels. For comparison, prior to the application of Zn^{2+}, only infrequent, fast transitions to the basal level of current were observed (Fig. 2*A*, control record). Furthermore, the frequency of spontaneous transitions between different smaller levels of conductance was greatly increased (Fig. 2*A*, middle records). Consistently, removal of Zn^{2+} from the trans compartment alone induced recovery of both the original conductance level and the pattern of activity with infrequent transitions (Fig. 2*A*, lower record).

From these data we generated open-channel current amplitude histograms for I–V curves (Fig. 1*C*). Since most transitions occurred between consecutive conductance levels, to estimate the fraction of time (FT) spent at any level of conductance, we counted the transitions between consecutive conductance levels as partial closures. These are plotted as a function of transmembrane potential in Fig. 2*B*. The frequency of brief transitions on the AβP[1–40] channel, evaluated in terms of the corresponding FT, appears to be rather insensitive to the transmembrane potential, both in the absence (●) and the presence (□) of Zn^{2+}. Indeed, under control conditions, FT_{110} and FT_{82} remained unchanged at *ca.* 0.98 (●) and at *ca.* 0.68 (□), respectively, even though the transmembrane potential was changed from −40 to 40 mV in 10-mV steps. The same voltage insensitivity applies to the FTs measured immediately after removal of Zn^{2+} (■). The decrease in FT, together with a marked decrease in AβP[1–40] channel conductance induced by Zn^{2+}, suggest that zinc

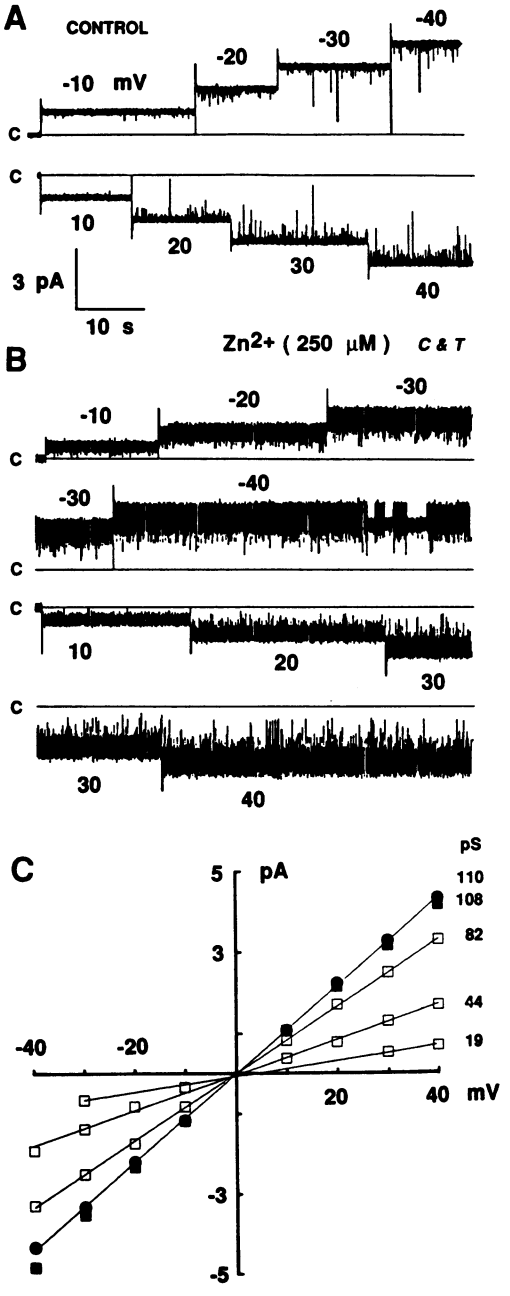

FIG. 1. Effects of transmembrane potential on gating and conductance blockade by Zn^{2+}. Recordings made in symmetrical 40 mM CsCl. (*A*) Under control conditions the membrane potential was varied, as indicated by the numbers near the corresponding record. (*B*) Records made a few minutes after the addition of small volumes of a 50 mM $ZnSO_4$ solution to both the cis and the trans compartments. Free [Zn^{2+}] was estimated as 250 μM. (*C*) I–V curves estimated from amplitude histograms. ●, Initial control; □, measurements made in the presence of Zn^{2+}; ■, final control minutes after replacement of the Zn^{2+}-containing solution by control solution (no $ZnSO_4$ added).

ions present in the solution can interact with the AβP[1–40] molecules in the bilayer. These effects were quite reversible, as illustrated by the fact that the conductance returned to 108 pS after removal of Zn^{2+} from the trans side (Figs. 1*C* and 2*A*, lower records).

Low Affinity Interactions Between Zn^{2+} and AβP[1–40] Channels of Low Conductance (<400 pS). The effects of increasing concentrations of Zn^{2+} on AβP[1–40] channel currents were measured in the presence of Zn^{2+} on both sides of the bilayer. For these experiments we selected those incorporations in which the

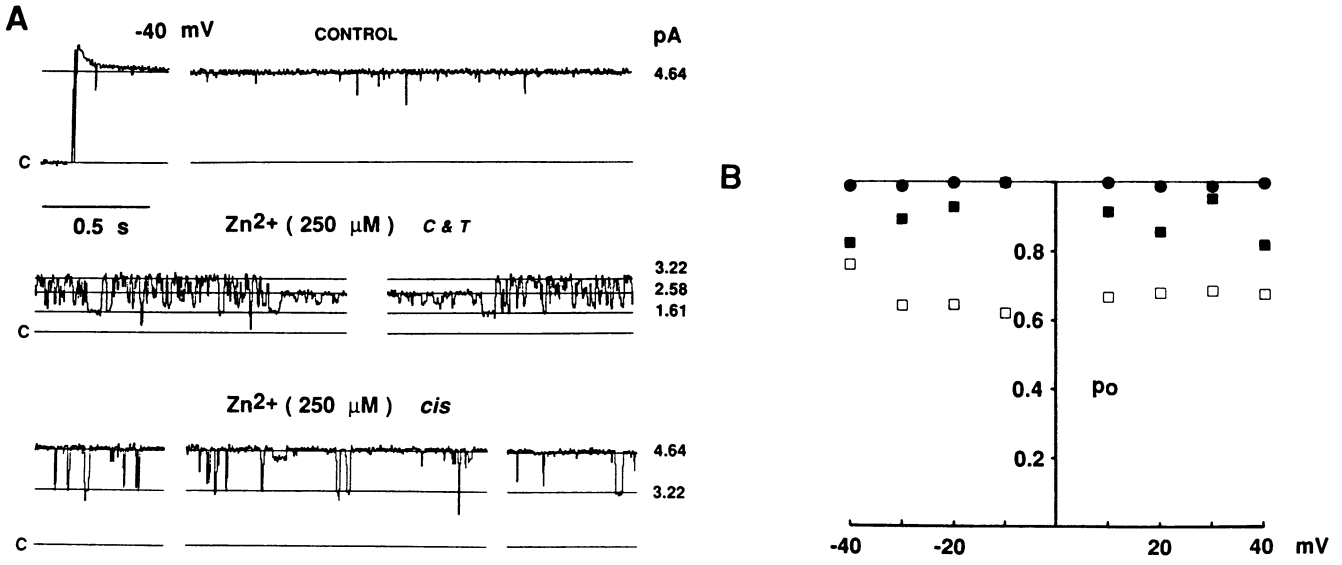

FIG. 2. Fast blockade by Zn^{2+} of AβP[1–40] channel gating expressed in terms of fractional open time. Recordings were made in symmetrical 40 mM CsCl. (*A*) Upper record: Segment of the record at −40 mV in Fig. 1*A* on an expanded time base. Middle records: Two segments from the record at −40 mV (expanded time base). Horizontal lines correspond to well-defined levels of the channel current. Values are given in pA next to the corresponding level. Bottom records: Three segments of the record made at −40 mV after removal of Zn^{2+} from the trans side. (*B*) Fractional time (FT) at the 82-pS level of conductance. Symbols are the same as for Fig. 1*C*.

AβP[1–40] channel activity was in the low conductance modality (i.e., <400 pS). As illustrated in Fig. 3 (upper records on the left and segment a on the right), no transitions to levels below 225 pS occurred during the entire record shown (*ca.* 3 min). Under these control conditions, the fraction of time the AβP[1–40] channel was found at its lowest level of conductance was *ca.*

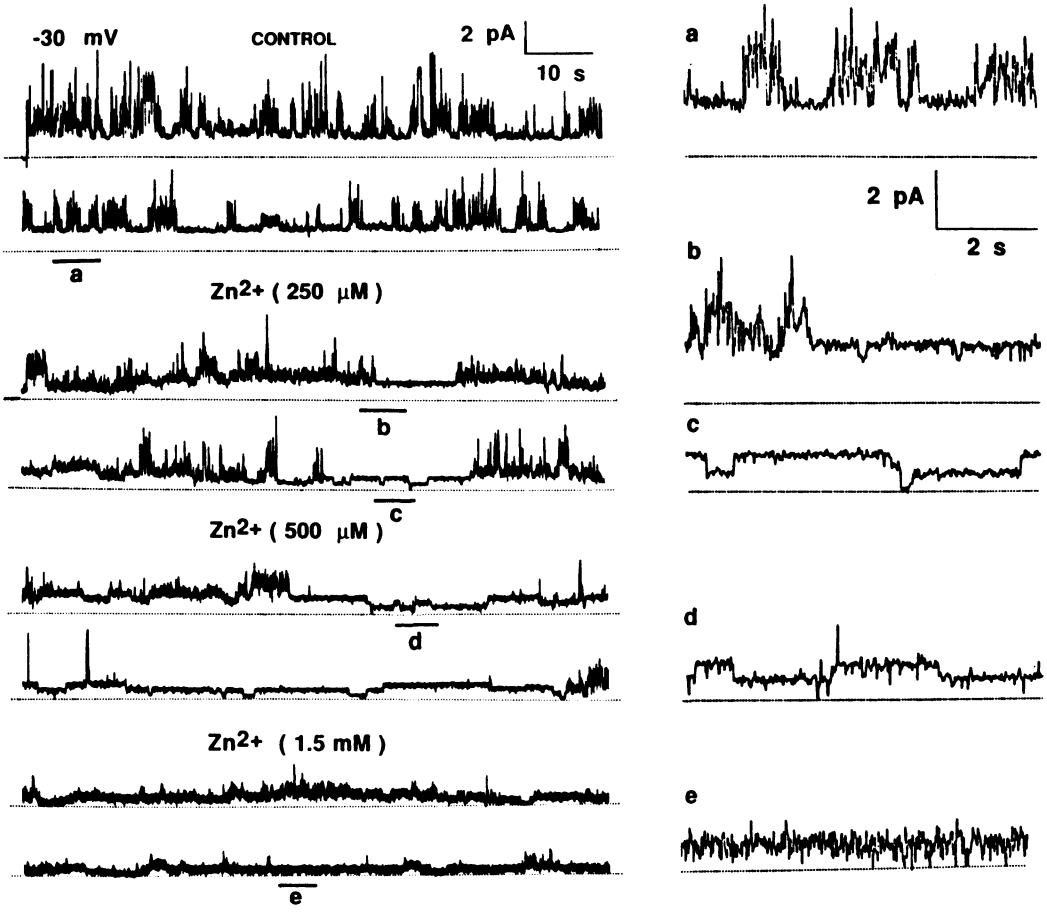

FIG. 3. Blockade of the AβP[1–40] channel in the low conductance modality by increasing concentrations of Zn^{2+}. (*Left*) Two segments of the control record are shown on the upper part. Segment a (indicated by the horizontal bar) is also shown on the right side using an expanded scale. Third and fourth records were made minutes after the addition of $ZnSO_4$ to achieve a concentration of *ca.* 250 μM; segment b is also shown on the right. Fifth and sixth records were made at 500 μM Zn^{2+}; segment d is shown on the right. Seventh and eighth records were obtained in the presence of 1.5 mM Zn^{2+}.

0.5. A few minutes after the application of Zn^{2+} (250 μM), there was a significant decrease in the frequency of the transitions to conductance levels above 225 pS. Furthermore, the direction of transitions changed in the opposite direction (Fig. 3, segment b), and transitions to a lower level of 88 pS began to occur (Fig. 3, segment c). On average, the fraction of time at 225 pS fell to 0.14. After a further increase in Zn^{2+} concentration to 500 μM, the FT below the 225-pS level of conductance was found to be 0.3. Under these conditions FT at the 88-pS level increased and complete AβP[1–40] channel closures were apparent (Fig. 3, segments d and e). At a Zn^{2+} concentration of 1.5 mM the 225-pS level of conductance was no longer observed, and channel currents exhibited high frequency flicker toward the closed level. An upper EC_{50} value of Zn^{2+} of *ca.* 300 μM was estimated from the change in FTs as a function of [Zn^{2+}].

Zn^{2+} Blockade of the Giant Conductance AβP[1–40] Channel (>400 pS). Single AβP[1–40] channel records are displayed at different transmembrane potentials in the giant conductance modality in Fig. 4 *A–C*. In symmetrical 40 mM K^+ a plot of the maximum values of the channel current as a function of potential could be fit by a straight line with slope of 4.7 nS (Fig. 4*D*, ●). Application of Zn^{2+} (500 μM) to the trans side induced a profound decrease in the amplitude of the channel current (Fig. 4*C*). These values were again linearly related to transmembrane potential, the slope of the regression line being equal to 197 pS (Fig. 4*D*, □). Spontaneous, discrete transitions between different levels of conductance continued to occur during the time course of the establishment of the blockade by Zn^{2+}. These transitions at −3, −2, and −1 mV are depicted in Fig. 4*B*. A segment from this record (indicated by the horizontal bar) is also shown beneath on an expanded time base. At least four levels (indicated by horizontal lines) are immediately apparent. The AβP[1–40] channel currents, after 4–5 min of exposure to Zn^{2+}, are shown in Fig. 4*C*. From these data we conclude that AβP[1–40] channels of large conductance are also blocked by Zn^{2+} but to a lesser extent at any given Zn^{2+} concentration. Taken together these results demonstrate that AβP[1–40] molecules in the bilayer can acquire multiple conformations that allow direct interaction between Zn^{2+} with some critical domains of the AβP[1–40] channel.

Spontaneous Conductance Transitions in Giant AβP[1–40] Channels. Zn^{2+} interactions with AβP[1–40] channels are characterized by an increased incidence of conductance transitions in both the low and the giant modalities. However, such conductance transitions are also seen in the absence of Zn^{2+}. The current records shown in Fig. 5 illustrate such transitions from three different experiments in either 40 mM CsCl (Fig. 5*A*, a–d) or symmetrical 140 mM KCl (Fig. 5*B*, a–d). The experiment in Fig. 5*A* shows a continuous recording at −1 mV, which is briefly interrupted by a 7-sec voltage increase to −10 mV. A wide range of current jumps is evident at both voltage levels, corresponding to conductance transitions ranging from 165 pS to 1.9 nS. Although the fluctuations are large, each conductance seems very stable, and the channel closes completely from either the lowest or highest conductance levels. In the experiments shown in Fig. 5*B*, segments a and b are from a continuous recording of a AβP[1–40] channel activity in which the voltage was changed from −1 to 2 mV. The initial conductance in Fig. 5*B*, a, begins at 168 pS and slowly stair-steps up to 1.08 nS over a 6-min period. When the polarity of the voltage is reversed (Fig. 5*B*, b) the conductance of the channel returns to a lower value of 300 pS with frequent brief transitions to a higher 420-pS value. In a different experiment shown in records 5, c and d, a similar stair-step occurs from 120 pS to 1.45 nS. The final examples show high frequency flickering between extremes in the conductance range Fig. 5*B*, b, with a 2-mV driving force, and Fig. 5*B*, d, with driving forces of −2 and −4 mV. These data, taken together, indicate that the

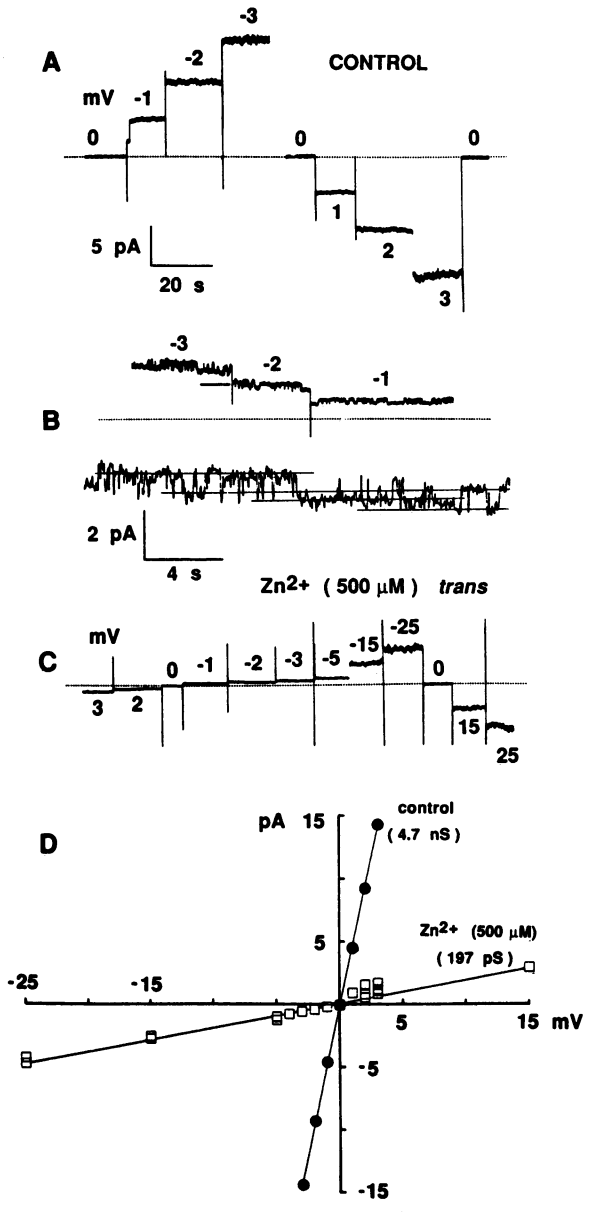

FIG. 4. Zn^{2+} blockade of the AβP[1–40] channel in the giant conductance modality. (*A*) Control records made in symmetrical 40 mM KCl solutions and in the absence of Zn^{2+} (slope conductance, 4.7 nS). (*B*) The development of the blockade was followed in time. Upper record (at −3, −2, and −1 mV): represents the status of the blockade by Zn^{2+} *ca.* 3 min after the addition of Zn^{2+} (500 μM) to the trans side of the bilayer chamber. The segment indicated by the horizontal bar is displayed on an expanded time base below. The horizontal lines indicate distinct levels of the channel current. (*C*) AβP[1–40] channel current at different transmembrane potentials acquired several minutes after the addition of Zn^{2+} (500 μM). (*D*) I–V curves during control conditions (●; slope conductance, 4.7 nS) and after stationary blockade (□; 197 pS).

jumps in conductance are more likely to be due to conformational transitions within the preassembled oligomeric channel than to the sequential addition of new monomeric units. Although such transitions occur spontaneously, as shown here, the addition of Zn^{2+} makes the transitions more apparent. This suggests that Zn^{2+} acts by favoring the manifestation of low conductance conformations.

Reversal of the Zn^{2+} Blockade by the Complexing Agent *o*-Phenanthroline. Replacement of the Zn^{2+}-containing 40 mM CsCl solution by 40 mM CsCl alone in the trans side (Fig. 2) leads

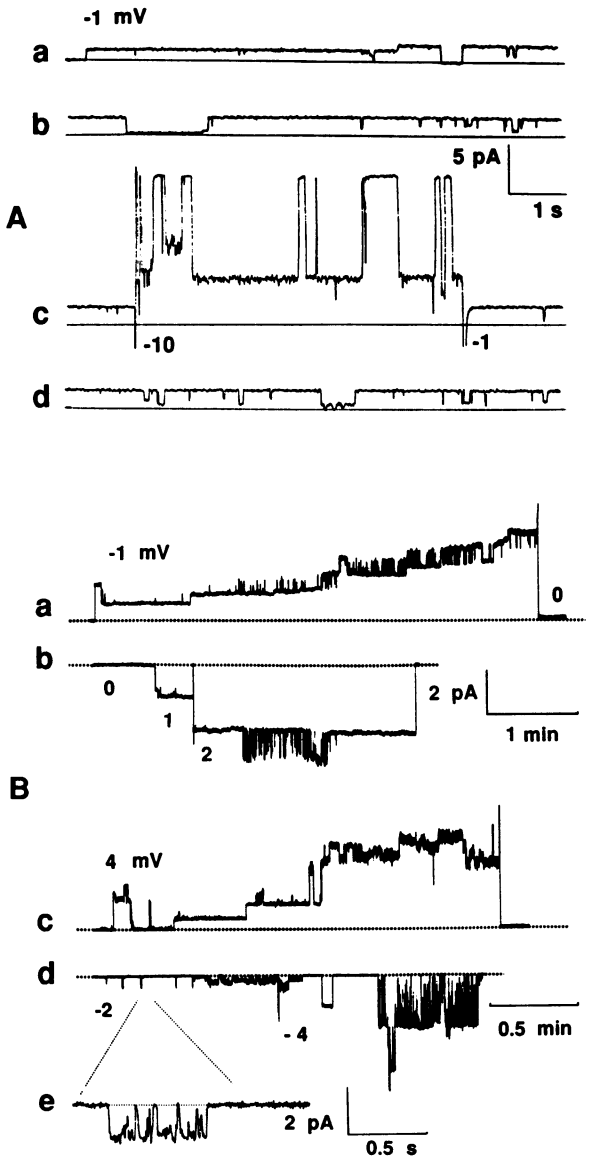

FIG. 5. Spontaneous AβP[1–40] channel transitions among low and giant levels of conductance. (*A*) Recordings made in symmetrical 40 mM CsCl solutions. Channel conductance at −1 mV along record a abruptly changed as follows: 0, 1280, 1050, 0, 1880, 0, 1900, 880, 1900, 680, 1900 pS. Similar transitions were observed at −10 mV (record c). (*B*) Recordings made in symmetrical 140 mM KCl solutions. Record a illustrates successive staircase-type transitions at −1 mV. Switching the potential to 2 mV (record b) induced regular transitions between two defined levels of conductance. Records c and d are from a different experiment under the same conditions. Segment e depicts the brief events observed at the beginning of record d at −2 mV.

to complete recovery of the original pattern of AβP[1–40] channel activity. We have also tested the Zn^{2+}-complexing chelator agent *o*-phenanthroline, with similar results. As illustrated in Fig. 6, application of Zn^{2+} (150 μM) to one of the sides (the cis side, in this case) evoked the expected, profound inhibition of the AβP[1–40] channel (Fig. 6, records in the middle). The Zn^{2+}-sensitive side can be either cis or trans because the initial incorporation of peptides by sonication in liposomes is random. This Zn^{2+} blockade was readily reversed by the addition of *o*-phenanthroline (200 μM) to the cis side containing the zinc.

DISCUSSION

We have shown here that Zn^{2+} interacts with specific domains of the AβP molecules by influencing ion conduction through

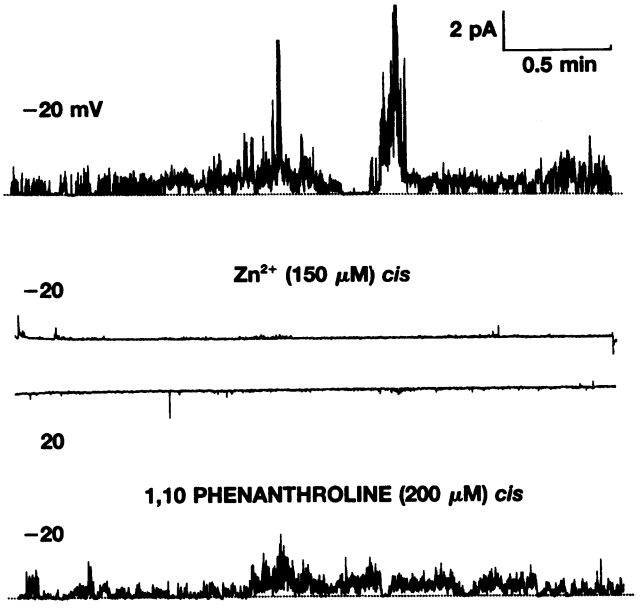

FIG. 6. *o*-Phenanthroline reverts the blockade of the AβP[1–40]-channel by Zn^{2+}. Recordings made in symmetrical 200 mM Cs glutamate. AβP[1–40] channel current observed in control conditions at −20 mV (upper record) is inhibited in both directions (−20 and 20 mV) by addition of Zn^{2+} (150 μM) to the cis side (records in the middle). AβP[1–40] channel activity is recovered after addition of *o*-phenanthroline (200 μM) to the cis side containing the Zn^{2+} (bottom record).

the AβP[1–40] channel pore. The interactions between Zn^{2+} present in the solution and AβP[1–40] channels inserted in the bilayer were expressed as profound changes in the frequency of spontaneous transitions between levels of AβP[1–40] channel current. Since the concentration of Zn^{2+} required to achieve measurable and reversible effects varied from 50 to 1500 μM, we conclude that at least one relatively low affinity (EC_{50} value of <300 μM) Zn^{2+}-binding domain is associated with the AβP[1–40] channel structure.

Zn^{2+} AβP[1–40] Channel Interactions Occur Outside the Membrane Electric Field. The profound increase in the frequency of brief closures induced by the application of $ZnCl_2$ (Fig. 1*B*) remained unchanged at different transmembrane potentials. Indeed, AβP[1–40] channel gating, evaluated in terms of the fraction of time spent at any level of conductance, appears to be insensitive to the transmembrane potential (Fig. 2*B*), in both the absence and the presence of Zn^{2+}. Since the frequency of the transitions between conductance levels also remained unchanged at different transmembrane potentials from −40 to 40 mV, we can conclude that the Zn^{2+}–AβP[1–40] interactions must occur at the entrance of the AβP[1–40] channel where the electric field is relatively constant.

We presume that the AβP[1–40] channel is a complex of peptides since the amyloid molecules are polymeric in their initial state in water (18, 26), and molecular modeling indicates that stable complexes could be formed by oriented polymers of AβP[1–40] in the membrane (17). It is thus worth considering the molecular basis of the different conductance states (Fig. 1). By analogy with the alamethicin system (14), different AβP[1–40] polymers could be responsible for the different conductance states (17). Alternatively, the different conductance states could be due to rapid interconversion among different conformations of the same AβP[1–40] polymer (28). All conductance levels appear to interconvert with each other, with high frequency flickering between two preferred conductance levels (Figs. 2 and 5), and, although less frequently observed, with the zero conductance level. Conventionally we

interpret this to indicate that a single channel with multiple conductance states is responsible for all of the data.

Possible Localization of the AβP[1–40] Channel Zn^{2+}-Binding Domain. The present results demonstrate that synthetic AβP[1–40] channels can assume a conformation that enables Zn^{2+} to interact asymmetrically with specific low affinity binding domains in the environment of the conducting pathway. However, sequence identification of the domain(s) involved remains to be determined. The predicted β-hairpin region of the AβP channel (17) contains three histidines (His_6, His_{13}, and His_{14}) and several nearby negatively charged residues (Asp_7 and Glu_{11}). These structural features are known to be essential for the association of Zn^{2+} with different metalloproteases (18–24). The best example of this mechanism is the enzyme involved in degrading internalized insulin. This Zn^{2+}-binding protease has an HXXEH Zn^{2+}-binding motif which is necessary for both catalytic activity and structural stabilization (18). However, the exact arrangement of the histidines and anionic residues is not crucial since some other Zn^{2+}-dependent metalloendoproteases have an inverted motif, HEXXH (19). In AβP[1–40] two Zn^{2+}-binding sites ($K_a^1 = 0.1$ and $K_a^2 = 5.2$ μM) have been recently reported experimentally (25). Indeed, from the perspective of the primary structure of AβP[1–40] there do exist two separate local sequences containing histidine. However, none of these precisely occurs in the metalloendoprotease motif. One contains His_6 in the local sequence of FRHDS, while the other contains His_{13} and His_{14} in the local sequence of EVHHQ. Nonetheless, when the peptide forms the predicted oligomeric channel structure in the membrane (17), the channel has predicted rings of His_6s and Asp_7's encircling one pore entrance. The other entrance is encircled by succeeding rings of Glu_{11}'s, His_{13}'s, and His_{14}'s. This theoretical asymmetry in putative Zn^{2+} binding sites would therefore appear to be correlated with the observed experimental asymmetry of the channel in terms of sensitivity to Zn^{2+}. The specific location of these sites is also consistent with the lack of voltage dependence of the Zn^{2+} block.

The interaction between Zn^{2+} and the AβP[1–40] has been characterized in previous studies in terms of the ability of Zn^{2+} to cause global polymerization of the peptide (25, 32). Since peptide polymerization has been implicated in the formation of the toxic form of the peptide, Zn^{2+} has been viewed as a negative factor in the genesis of AD (25). On the other hand, the ability of the peptide to assemble into oligomeric complexes possessing giant cation channels properties has been suggested as the basis of amyloid neurotoxicity (13–16). From the latter perspective, our present experiments showing that Zn^{2+} has the ability to interact with and block the AβP[1–40] channel conductance could thus be construed as protective. The interactions of Zn^{2+} with amyloid peptide may thus be multiple, and one consequence of these interactions could even lead to attenuation of amyloid channel neurotoxicity.

1. Neve, R. L., Dawes, L. R., Yankner, B. A., Benowitz, L. I., Rodriguez, W. & Higgins, G. A. (1990) *Prog. Brain Res.* **86,** 257–267.
2. Hardy, J. A. & Higgins, G. A. (1992) *Science* **256,** 184–185.
3. Selkoe, D. J. (1991) *Neuron* **8,** 487–496.
4. Roth, M., Tomlinson, B. E. & Blessed, G. (1966) *Nature (London)* **209,** 109–110.
5. Joachim, C. L., Duffy, L. K. & Selkoe, D. (1988) *Brain Res.* **474,** 100–111.
6. Masters, C. L., Simms, G., Weinman, N. A., Multhaup, G., McDonald, B. L. & Beyreuther, K. (1985) *Proc. Natl. Acad. Sci. USA* **82,** 4245–4249.
7. Goldgaber, D., Lerman, M. I., McBride, O. W., Saffiotti, U. & Gajdusek, C. (1987) *Science* **235,** 877–880.
8. Tanzi, R. E., Gusella, J. F., Watkins, P. C., Bruns, G. A. P., St. George-Hyslop, P., Van Keuren, M. L., Patterson, D., Pagan, S., Kurnit, D. M. & Neve, R. L. (1987) *Science* **235,** 880–882.
9. Yankner, B. L., Duffy, L. K. & Kirschner, D. A. (1990) *Science* **250,** 279–282.
10. Kowall, N. C., McKee, A. C., Yankner, B. A. & Beal, M. F. (1992) *Neurobiol. Aging* **13,** 537–542.
11. Malouf, A. T. (1992) *Neurobiol. Aging* **13,** 543–551.
12. Yankner, B. A. (1992) *Neurobiol. Aging* **13,** 615–616.
13. Arispe, N., Rojas, E. & Pollard, H. B. (1993) *Proc. Natl. Acad. Sci. USA* **90,** 567–571.
14. Arispe, N., Pollard, H. B. & Rojas, E. (1993) *Proc. Natl. Acad. Sci. USA* **90,** 10573–10577.
15. Arispe, N., Pollard, H. B. & Rojas, E. (1994) *Ann. N.Y. Acad. Sci.* **747,** 256–266.
16. Arispe, N., Pollard, H. B. & Rojas, E. (1994) *Mol. Cel. Biochem.* **140,** 119–125.
17. Durell, S. R., Guy, H. R., Arispe, N., Rojas, E. & Pollard, H. B. (1994) *Biophys. J.* **67,** 2137–2145.
18. Perlman, R. K. & Rosner, M. R. (1994) *J. Biol. Chem.* **269,** 33140–33145.
19. Brzovic, P. S., Choi, W. E., Borchardt, D., Kaarsholm, N. C. & Dunn, M. F. (1994) *Biochemistry* **33,** 13057–13069.
20. Becker, A. B. & Roth, R. A. (1993) *Biochem. J.* **292,** 137–142.
21. Ciszak, E. & Smith, G. D. (1994) *Biochemistry* **33,** 1512–1517.
22. Jacoby, E., Kruger, P., Karatas, Y. & Wollmer, A. (1993) *Biol. Chem. Hoppe Seyler* **374,** 877–885.
23. Gehm, B. D., Kuo, W. L., Perlman, R. K. & Rosner, M. R. (1993) *J. Biol. Chem.* **268,** 7943–7948.
24. Gross, L. & Dunn, M. F. (1992) *Biochemistry* **31,** 1295–1301.
25. Bush, A. I., Pettingell, W. H., Paradis, M. D. & Tanzi, R. E. (1994) *J. Biol. Chem.* **269,** 12152–12158.
26. Bush, I., Multhaup, G., Moir, R. D., Williamson, T. G., Small, D. H., Rumble, B., Pollwein, P., Beyreuther, K. & Masters, C. L. (1993) *J. Biol. Chem.* **268,** 16109–16112.
27. Kuroda, Y. & Kawahara, M. (1994) *Tohoku J. Exp. Med.* **174,** 263–268.
28. Pollard, J. R., Arispe, N., Rojas, E. & Pollard, H. B. (1994) *Biophys. J.* **67,** 647–655.
29. Hyman, B. T., Van Hoesen, G. W., Kroner, L. J. & Damasio, A. R. (1986) *Ann. Neurol.* **20,** 472–481.
30. Frederickson, C. J. (1989) *Int. Rev. Neurobiol.* **31,** 145–328.
31. McLachlan, D. R., Fraser, P. E. & Dalton, A. J. (1992) *Ciba Found. Symp.* **169,** 87–98; Discussion 99–108.
32. Kawahara, M., Muramoto, K., Kobayashi, K., Mori, H. & Kuroda, Y. (1994) *Biochem. Biophys. Res. Commun.* **198,** 531–535.